SU(4) lattice gauge theory with decuplet fermions: Schrödinger functional analysis

Thomas DeGrand, Yigal Shamir, and Benjamin Svetitsky

SU(4) lattice gauge theory with decuplet fermions: Schrödinger functional analysis

Thomas DeGrand

Department of Physics, University of Colorado, Boulder, CO 80309, USA

Yigal Shamir and Benjamin Svetitsky

Raymond and Beverly Sackler School of Physics and Astronomy, Tel Aviv University, 69978 Tel Aviv, Israel

We complete a program of study of SU(N) gauge theories coupled to two flavors of fermions in the two-index symmetric representation by performing numerical simulations in SU(4). The beta function, defined and calculated via the Schrödinger functional, runs more slowly than the two-loop perturbative result. The mass anomalous dimension levels off in strong coupling at a value of about 0.45, rendering this theory unsuitable for walking technicolor. A large-N comparison of these data with results from SU(2) and SU(3) reveals striking regularities.

I. INTRODUCTION

In the last few years there has been an explosion of interest in lattice simulations of theories with gauge fields coupled to a large number of fermionic degrees of freedom, either many flavors of fermions in the fundamental representation or a few flavors of fermions in higher-dimensional representations of the gauge group [1]. The primary motivation to study these models is their potential use as technicolor theories—extensions to electroweak theory with no fundamental Higgs field [2]. To be a viable candidate, a theory must exhibit spontaneous symmetry breaking, providing Goldstone bosons to be eaten by the electroweak gauge bosons. It must also have a slowly running gauge coupling and a mass anomalous dimension γ_m near unity, in order to give realistic masses to Standard Model fermions while correctly suppressing flavor-changing neutral currents.

Expectations for candidate theories, based on the two-loop beta function, are easily stated [3, 4]. Too many fermionic degrees of freedom render the Gaussian fixed point infrared stable. With a smaller number of fermionic fields, asymptotic freedom returns but the beta function possesses a zero, signaling the presence of an infrared-attractive fixed point (IRFP). Theories with IRFP's are said to reside within a "conformal window" in the (N_c, N_f) plane, wherein the IR physics displays conformal invariance and no particle spectrum. The fermion mass is then a relevant parameter whose presence induces a mass gap. Further decreasing the number of fermion fields takes us out of the conformal window to the QCD-like domain of confinement and chiral symmetry breaking. Just outside the conformal window, there may be a borderland where the beta function approaches zero without actually crossing it; this gives candidates for "walking technicolor," where the running coupling comes to a near-standstill for many decades in the energy scale, until chiral symmetry breaking eventually sets in.

This paper presents a study of the running gauge coupling and mass anomalous dimension for SU(4) gauge fields coupled to two flavors of decuplet fermions, that is, fermions in the two-index symmetric representation. It is a continuation of our previous work on SU(2) and SU(3) gauge theories with fermions in the corresponding representations [5–11]. Recent interest in these models dates from the proposal by the authors of Refs. [12, 13] that they might make good technicolor candidates. All three theories possess two-loop IRFP's, raising the possibility that they might become walking theories when studied nonperturbatively. In addition, the small number of flavors was seen as favorable from the point of view of evading precision electroweak constraints.

Using the Schrödinger functional (SF) method [14–22], we were able to confirm an IRFP in the SU(2) theory, placing it within the conformal window [9]; our most recent result for the SU(3) theory was the same, but at a lower level of statistical confidence [11]. Our calculations of γ_m allowed a strong claim, in both cases, that γ_m levels off at strong coupling so that it never exceeds 0.45; thus neither theory can be used for walking technicolor, regardless of the existence of the IRFP. In an effort to find a phenomenologically viable theory with $\gamma_m \simeq 1$, we turn to the SU(4) theory. Our motivation for this lies in the one-loop expression for γ_m,

$$\gamma_m = \frac{6C_2(R)}{16\pi^2} g^2, \qquad (1)$$

which is proportional to the quadratic Casimir operator $C_2(R)$ of the fermion representation; in going from the sextet SU(3) theory to decuplet SU(4), $C_2(R)$ increases from 10/3 to 9/2, or 35%. If the non-perturbative result were to follow this pattern then a value near 1 would be within reach.

As in our earlier work, we apply the SF method to calculate the nonperturbative beta function. The original method yields a discrete analogue of the beta function that gives the change in the running coupling when the length scale changes by a fixed ratio. We have noted [9] that when the coupling runs slowly, as it does in the theories at hand, an approximate result for the usual beta function can be obtained directly. SF techniques also allow one to measure γ_m from the volume dependence of

Z_P, the renormalization factor of the pseudoscalar density $\bar{\psi}\tau^a\gamma_5\psi$.[1]

Analyzing these theories via numerical simulations presents a different set of problems than is seen in QCD [31]. The major new feature is the slow running of the coupling. As we have noted, the slow running simplifies much of the analysis, both of the beta function and of γ_m. On the other hand, it is difficult to tell a slowly running coupling from one that does not run at all, so that the location of any IRFP may be poorly determined. The main problem with slow running, however, is that if the bare coupling is tuned to be strongly interacting at long distance, then it will be strongly interacting at short distance. This raises the possibility of strong lattice artifacts, in particular the appearance of unphysical phase transitions.

Such a transition is present in all our candidate theories. Our lattice simulations use fermions with a Wilson-type discretization, which breaks chiral symmetry. Simulations are done at zero quark mass, but the quark mass is a derived quantity, determined from the axial Ward identity. Reaching zero fermion mass involves tuning the hopping parameter at fixed bare coupling. At strong coupling a lattice transition occurs, and when it does, nowhere does the fermion mass vanish. Instead, it jumps discontinuously from positive to negative value. The absence of a massless theory in strong coupling makes it impossible to apply the SF method there. To evade this problem, we change the lattice discretization to push the transition away from the region of bare parameter space where we wish to run.

Our result for the beta function is similar to what we found in the triplet SU(2) and sextet SU(3) theories. The nonperturbative result is consistently smaller in magnitude than the two-loop estimate, but in this case, as in SU(3), we cannot state definitely that it crosses zero. The result for γ_m follows closely the pattern of the other two theories: It follows the perturbative line, Eq. (1), for weak coupling but departs from it and saturates at $\gamma_m \simeq 0.45$ (see below for error estimates).

The outline of the paper is as follows. In the next section we describe our generalized lattice action, formulated to suppress lattice artifacts in the strong-coupling region. In Sec. III we present our results for the beta function and in Sec. IV the mass anomalous dimension. Since we now hold results for the SU(N) theories with $N = 2$, 3, and 4, we can discuss them in the language of large-N gauge theories; we show in Sec. V that the consistency of the three theories is remarkable. The appendices present our method of smearing gauge links in SU(4), perturbative and nonperturbative tests of our gauge action, and a tabulation of our simulation ensembles.

II. GENERALIZING THE LATTICE ACTION

We study the SU(4) gauge theory coupled to two flavors of dynamical fermions in the symmetric representation (the decuplet) of the color gauge group. Our techniques are mostly identical to our previous work with the SU(2) and SU(3) theories [9, 11]. We have already used a generalized gauge action for the SU(3) theory; here we give a more thorough discussion.

We use the Wilson fermion action with added clover term [32]. The gauge connections in the fermion action are defined with a differentiable hypercubic (nHYP) smearing [33, 34] of the fundamental links, from which the decuplet gauge connection for the fermion operator is constructed.[2] We began this project with the usual single-plaquette Wilson gauge action. The parameters that are inputs to the simulations are the gauge coupling $\beta = 8/g_0^2$ and the fermion hopping parameter κ, related to the bare mass m_0 by $\kappa = (8 + 2m_0)^{-1}$. The clover coefficient is set to its tree-level value of unity.

The Schrödinger-functional study of the running coupling is carried out at zero fermion mass, which defines the critical hopping parameter $\kappa_c(\beta)$. We define the fermion mass m_q and its related critical hopping parameter κ_c through the axial Ward identity (AWI),

$$\partial_t \sum_{\mathbf{x}} \langle A_0^a(\mathbf{x}, t)\mathcal{O}^a \rangle = 2m_q \sum_{\mathbf{x}} \langle P^a(\mathbf{x}, t)\mathcal{O}^a \rangle, \quad (2)$$

where the axial current $A_\mu^a = \bar{\psi}\gamma_\mu\gamma_5(\tau^a/2)\psi$, the pseudoscalar density $P^a = \bar{\psi}\gamma_5(\tau^a/2)\psi$, and $\mathcal{O}^a$ is a gauge-invariant wall source at $t = a$. (See [8] for more details.) With the simplest lattice action—the single-plaquette gauge action and thin-link Wilson fermions—it turns out to be impossible to set the fermion mass to zero when the gauge coupling is strong. In that regime there is a first-order phase boundary at which the AWI mass jumps across zero as κ is adjusted, never taking the value zero. Thus there is no place where the fermions are massless in strong coupling: The κ_c line simply terminates. This has been observed in theories with many Wilson-type fermions—many fundamental flavors [35–37], or a few flavors of higher-representation fermions [8, 38, 39]. For our purposes, this phase transition prevents the extension of the SF calculation to strong coupling.

The transition is a lattice artifact. Its location can be shifted by changing the lattice action. For triplet SU(2) with $N_f = 2$, SF calculations with thin-link fermions [25, 26] were hampered by this transition; with nHYP clover fermions we pushed the transition back and exposed the IRFP [9]. For SU(3) and SU(4) this change of action turns out to be insufficient and the first order transition remains at fairly weak coupling.

---

[1] For other applications of the SF method to technicolor candidates, see [23–30].

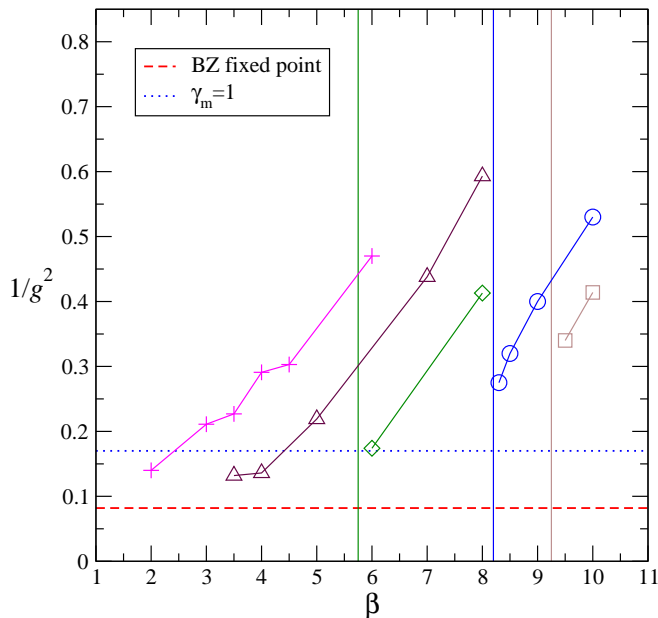[2] The extension of this smearing to the gauge group SU(4) is described in Appendix A.

FIG. 1: Inverse SF coupling versus gauge coupling β for several choices of β_{10}, measured with short runs on a 6^4 lattice. The connected data sets are for (right to left) $\beta_{10} = -0.5$, 0, 0.5, 1.0, 1.5. For the first three values of β_{10}, the vertical lines mark the appearance of the first-order transition that makes κ_c disappear for smaller β. The horizontal dashed line near the bottom of the graph marks the location of the Banks–Zaks (two-loop) fixed point. The horizontal dotted line marks where the one-loop $\gamma_m(g^2)$ is equal to unity.

We find that a modification of the *gauge* action can move the transition away and allow the study of stronger couplings. We supplement the original plaquette term with an additional plaquette term, constructed with the same link as is used in the fermion action—a fat link in the higher representation. The action is

$$S_G = \frac{\beta}{8} \sum \operatorname{Re} \operatorname{Tr} U_\mu(x) U_\nu(x + \hat{\mu}) U_\mu^\dagger(x + \hat{\nu}) U_\nu^\dagger(x)$$
$$+ \frac{\beta_{10}}{20} \sum \operatorname{Re} \operatorname{Tr} V_\mu(x) V_\nu(x + \hat{\mu}) V_\mu^\dagger(x + \hat{\nu}) V_\nu^\dagger(x),$$
$$(3)$$

where $U_\mu(x)$ is the thin link and $V_\mu(x)$ the fat link in the decuplet representation. We will refer to this action as a "soft gauge action."[3] We note that the fat plaquette term would appear in a hopping-parameter expansion in $O(\kappa^4)$; such an induced term has been blamed for the first-order phase boundary [38], so it makes sense to try to adjust its strength.

---

[3] We offer a perturbative analysis of soft gauge actions in Appendix B, as well as evidence that they do not negate the advantages of fattening the links in the fermion action.
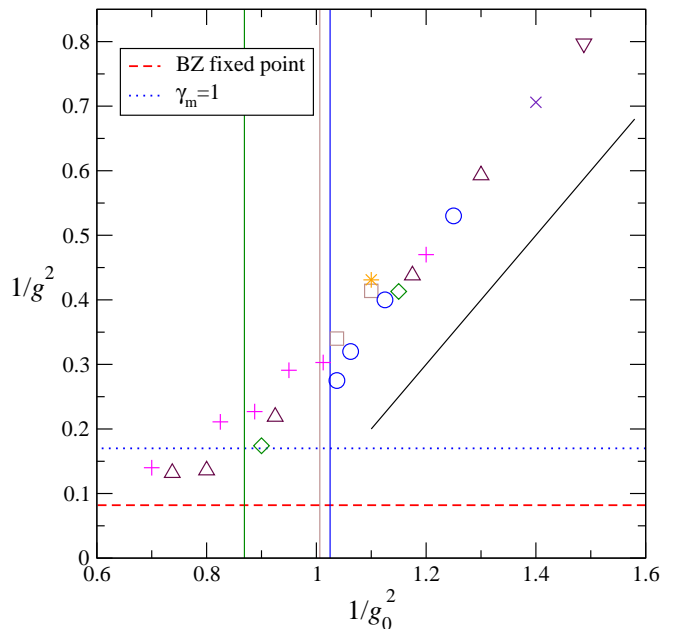

FIG. 2: Inverse SF coupling versus inverse bare coupling $1/g_0^2$ as defined in Eq. (4). Plotting symbols are as in Fig. 1, plus additional single points for $\beta_{10} = 2.0$ (star), $\beta_{10} = 3.0$ ($\times$), and $\beta_{10} = 3.5$ (triangle at the top). The diagonal line has unit slope.

The advantages of the soft gauge action can be seen in Fig. 1, a plot of the inverse SF coupling $1/g^2$ versus β for various values of β_{10}, measured on a fixed lattice size. Our goal is to investigate small values of $1/g^2$, in particular the neighborhood of the Banks–Zaks fixed point and of the coupling where the one-loop anomalous dimension $\gamma_m(g^2)$ is equal to unity. These are marked by the horizontal lines in the figure. The circles denote results for $\beta_{10} = 0$, meaning the original thin-link plaquette action. The vertical line just to the left of the leftmost circle marks the bare coupling where the first-order boundary appears and there is no κ_c. Thus one cannot investigate the region $1/g^2 \lesssim 0.25$ with the plaquette action. Increasing β_{10} pushes the phase transition to smaller β; as it turns out, this allows us to reach smaller values of $1/g^2$ before encountering the transition. For $\beta_{10} \gtrsim 1$ we can no longer find the transition in the coupling region we studied.

Having data from many lattice actions allows us to test universality, with the results shown in Fig. 2. We plot all the lattice data against the perturbative bare lattice coupling,

$$\frac{1}{g_0^2} = \frac{1}{8} \left(\beta + \frac{12}{5} \beta_{10} \right) \qquad (4)$$

[cf. Eq. (B3)]. The points indeed collapse to a common curve, especially in weak coupling. In perturbation theory, the bare and SF couplings are related by

TABLE I: Running coupling, Eq. (6), evaluated at the bare couplings $(\beta, \beta_{10}, \kappa_c)$ on lattices of size L. The omission of the result for $L = 16$ at $\beta = 5.0$ is explained in Appendix C.

β	β_{10}	$1/g^2$			
		$L = 6a$	$L = 8a$	$L = 12a$	$L = 16a$
10.0	0	0.5778(19)	0.5440(40)	0.5241(64)	–
9.0	0	0.4095(19)	0.3915(37)	0.3610(42)	0.3334(72)
8.5	0	0.3199(19)	0.2979(32)	0.2780(69)	–
7.0	1	0.4377(11)	0.4217(26)	0.4024(52)	–
6.0	1	0.3101(27)	0.3019(32)	0.2844(64)	–
5.0	1	0.2157(27)	0.2103(40)	0.2002(53)	*
4.5	1	0.1714(27)	0.1722(32)	0.1721(47)	0.1631(67)
4.0	1	0.1443(24)	0.1389(26)	0.1332(35)	0.1413(46)
3.5	1	0.1070(18)	0.1106(29)	0.1087(42)	–

$$g^2 = g_0^2 + C g_0^4 + \cdots, \text{ or}$$

$$1/g^2 = 1/g_0^2 - C + \cdots . \qquad (5)$$

The solid diagonal line is plotted to show that the slope of the data indeed approaches 1 in weak coupling.

III.   BETA FUNCTION

The computation of the running coupling proceeds as described in Ref. [8], with adaptations to the SU(4) case. We set boundary conditions on the gauge fields as described in [22], while the fermions obey the usual homogeneous boundary conditions at $t = 0, L$. The coupling emerges from a measurement of the derivative of the action with respect to a parameter η in the boundary gauge field,

$$\frac{K}{g^2(L)} = \left\langle \frac{\partial S_G}{\partial \eta} - \text{tr}\left(\frac{1}{D_F^\dagger} \frac{\partial (D_F^\dagger D_F)}{\partial \eta} \frac{1}{D_F} \right) \right\rangle \Bigg|_{\eta=0} . \qquad (6)$$

The constant K can be calculated from the derivative of the classical continuum action with respect to η, giving $K = -12\pi$. For details of the ensembles generated see Appendix C.

Our results for the running coupling are listed in Table I and plotted in Fig. 3. It is convenient to define the beta function $\tilde{\beta}(u)$ for $u \equiv 1/g^2$ as

$$\tilde{\beta}(1/g^2) \equiv \frac{d(1/g^2)}{d \log L} = \frac{2\beta(g^2)}{g^4} = 2u^2 \beta(1/u) \qquad (7)$$

in terms of the conventional beta function $\beta(g^2)$. As discussed in Ref. [9], the slow running of the coupling justifies extracting the beta function at each (β, κ_c) from a linear fit of the inverse coupling

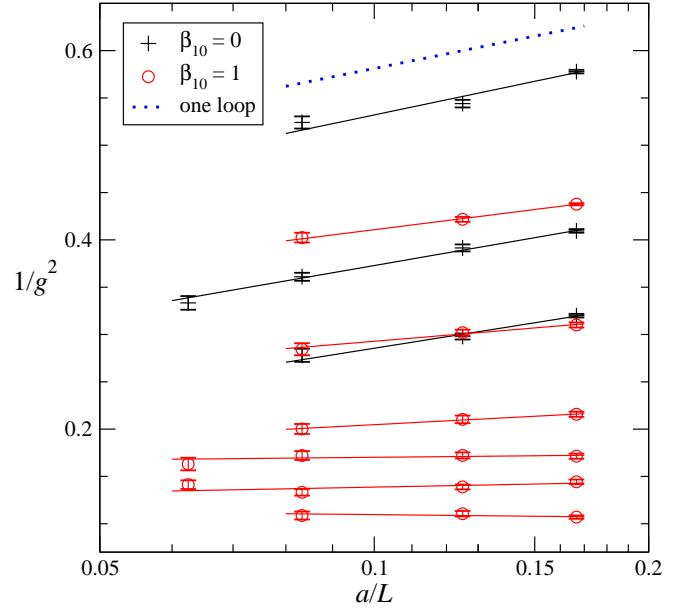$$u(L/a) = c_0 + c_1 \log \frac{L}{8a}. \qquad (8)$$

FIG. 3: Running coupling $1/g^2$ calculated on lattices of size L (see Table I). The crosses are from simulations with $\beta_{10} = 0$: top to bottom, $\beta = 10.0, 9.0, 8.5$. The circles are from simulations with $\beta_{10} = 1$: top to bottom, $\beta = 7.0, 6.0, 5.0, 4.5, 4.0, 3.5$. The straight lines are linear fits [Eq. (8)] to each set of points at given (β, β_{10}); the slope gives the beta function. The dotted line shows the expected slope from one-loop running.
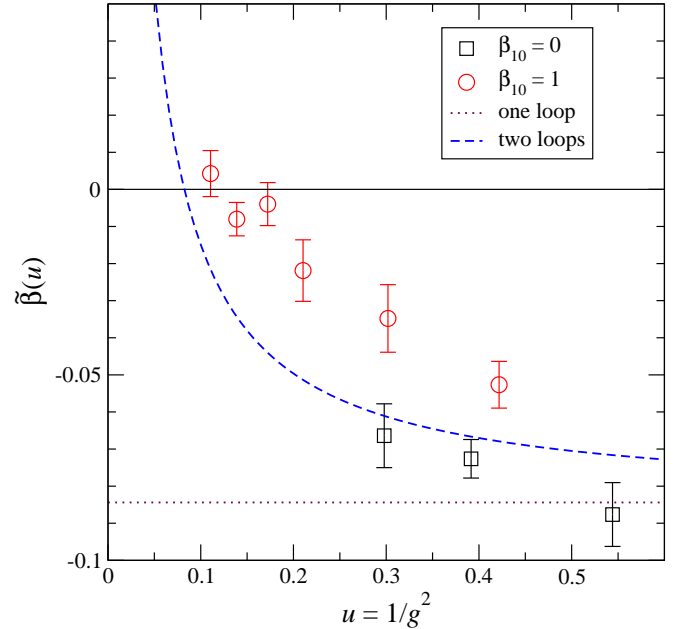

FIG. 4: Beta function $\tilde{\beta}(u)$ as extracted from the linear fits (8), plotted as a function of $u(L = 8a)$. The squares are from the $\beta_{10} = 0$ data while the circles are from $\beta_{10} = 1$. Plotted curves are the one-loop (dotted line) and two-loop (dashed line) beta functions.
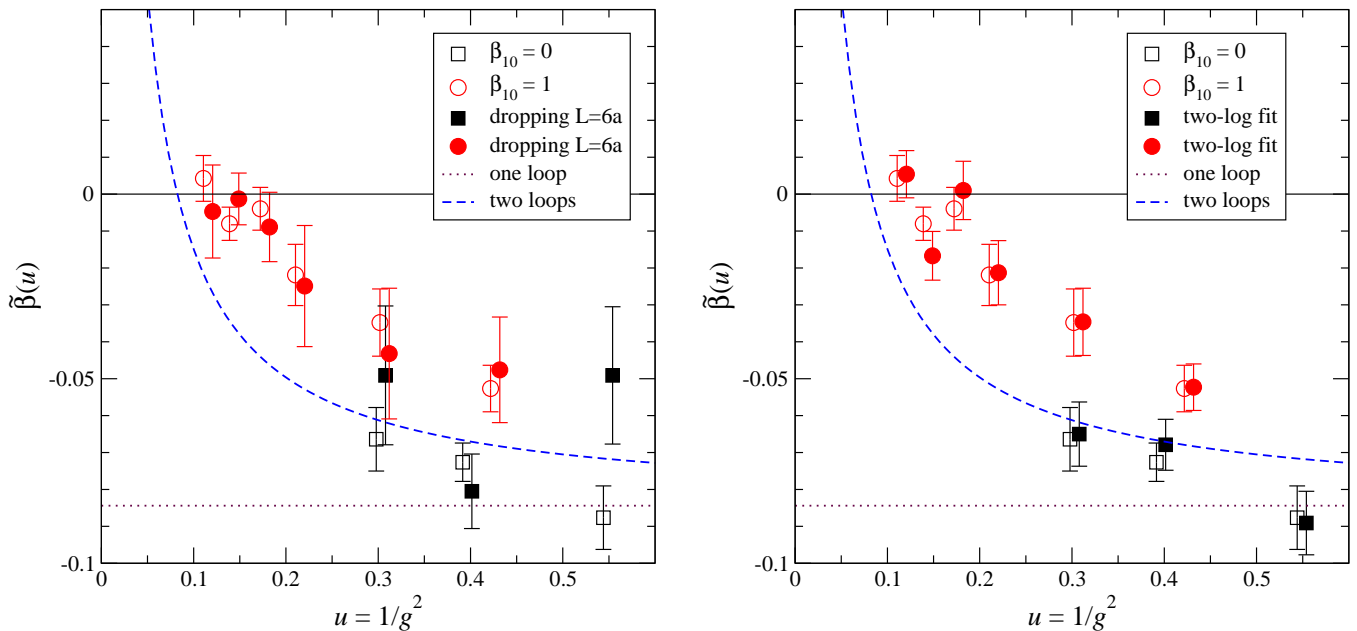
FIG. 5: Comparison of different fit types. Empty symbols as in Fig. 4. Left panel: full symbols derive from linear fits in which the $L = 6a$ points are omitted. Right panel: full symbols derive from fits to Eq. (10), in which a $\log^2$ term has been added. Results are plotted against $u(L = 8a)$. The filled symbols have been slightly displaced to the right.

c_1 is an estimate for the beta function $\tilde{\beta}$ at this coupling. These fits are shown in Fig. 3. Each fit was done using all the available volumes at the given bare parameters. Values of the beta function $\tilde{\beta}(u)$ obtained from these fits are plotted as a function of $u(L = 8a)$ in Fig. 4. There is some discrepancy between the results for $\beta_{10} = 0$ and those for $\beta_{10} = 1$; as we shall see, this discrepancy is not robust under changes of the fitting procedure. Also shown are the one- and two-loop approximations from the expansion

$$\tilde{\beta}(u) = -\frac{2b_1}{16\pi^2} - \frac{2b_2}{(16\pi^2)^2}\frac{1}{u} + \cdots , \qquad (9)$$

where $b_1 = 20/3$ and $b_2 = -260/3$.

The assumption behind the linear fits is that $\tilde{\beta}$ is small so that $u(L/a)$ changes very slowly with the volume; this behavior is apparent in Fig. 3. Indeed the fits have good χ^2, which justifies our hypothesis. Corrections to the simple model (8) come from discretization errors, as well as from the slight deviation from constancy of the continuum beta function over the range of volumes. Discretization errors have the form of powers of a/L. We have found that such corrections are only loosely constrained in a generalized fit; thus we prefer to estimate the uncertainty due to these corrections by redoing the linear fits while omitting the smallest lattice, $L = 6a$. The results are shown in the left-hand panel of Fig. 5. While the error bars have increased, on the whole the

results are stable.[4]

Deviations from constancy of the (continuum) beta function give rise to higher powers of $\log L/a$. Adding the next-to-leading term, at each bare coupling we fit

$$u(L/a) = c_0 + c_1 \log L/8a + c_2 (\log L/8a)^2. \qquad (10)$$

From the definition of the beta function it follows that c_1 continues to provide an estimate for the beta function at $u = 1/g^2(L = 8a)$. The results of these fits are shown in the right-hand panel of Fig. 5. This time there is hardly any change compared to the linear fits of Eq. (8).[5]

While the data trend towards a zero crossing, meaning an IRFP, we cannot confirm the existence of this crossing. It is possible that the beta function turns away from zero, resulting in a walking scenario. If the function does cross zero, we can offer an estimate of the crossing point. For each fit type, we determine the zero of the beta function from a linear fit of $\tilde{\beta}$ vs. u, using the $\beta_{10} = 1$ points. In fitting to any of Figs. 4–5, we find little difference whether we fit to 4, 5, or 6 points starting at the lowest u. Moreover, the three figures give nearly equal central values for the crossing, and comparable error bars. The largest 1σ interval covers all the others. Taking it as our

---

[4] Note that dropping $L = 6a$ for the cases where there are only three volumes leaves no degrees of freedom for the linear fit.

[5] Here, too, fitting the cases with only three volumes leaves no degrees of freedom for the fit.

TABLE II: Pseudoscalar renormalization factor Z_P evaluated at the couplings $(\beta, \beta_{10}, \kappa_c)$ for lattice sizes L.

β	β_{10}	Z_P			
		$L = 6a$	$L = 8a$	$L = 12a$	$L = 16a$
10.0	0	0.2210(3)	0.2011(6)	0.1754(7)	–
9.0	0	0.1852(4)	0.1618(4)	0.1324(4)	0.1168(6)
8.5	0	0.1565(4)	0.1331(5)	0.1066(7)	–
7.0	1	0.1869(2)	0.1682(3)	0.1473(4)	–
6.0	1	0.1652(5)	0.14617(35)	0.1243(7)	–
5.0	1	0.1452(4)	0.1283(5)	0.1066(7)	0.0955(5)
4.5	1	0.1357(4)	0.1187(4)	0.1006(6)	0.0895(10)
4.0	1	0.1266(4)	0.1095(5)	0.0921(7)	0.0813(4)
3.5	1	0.1150(4)	0.1019(4)	0.0835(6)	–

final uncertainty, we arrive at

$$6.5 \le g_*^2 \le 12 \qquad (11)$$

for the location of the supposed IRFP.

IV. MASS ANOMALOUS DIMENSION

We derive the mass anomalous dimension from the scaling with L of the pseudoscalar renormalization factor Z_P [8, 19–21, 26]. The latter is calculated by taking the ratio

$$Z_P = \frac{c\sqrt{f_1}}{f_P(L/2)}. \qquad (12)$$

f_P is the propagator from the a wall source at the $t = 0$ boundary to a point pseudoscalar operator at time $L/2$. The normalization of the wall source is removed by the f_1 factor, which is a boundary-to-boundary correlator. The constant c, which is an arbitrary normalization, is $1/\sqrt{2}$ in our convention.

We present the calculated values Z_P in Table II and plot them in Fig. 6. Again [9], the slow running suggests that we may attempt to extract γ_m from the approximate scaling formula

$$Z_P(L) = Z_P(L_0) \left(\frac{L_0}{L} \right)^\gamma, \qquad (13)$$

that is, from the slopes of the lines drawn in Fig. 6. These linear fits are analogous to Eq. (8):

$$\log Z_P(L/a) = c_0 + c_1 \log \frac{L}{8a}. \qquad (14)$$

The results are shown in Fig. 7. Similarly, we have also applied the linear fit with the smallest volume $L = 6a$ removed, and we considered a fit function analogous to Eq. (10),

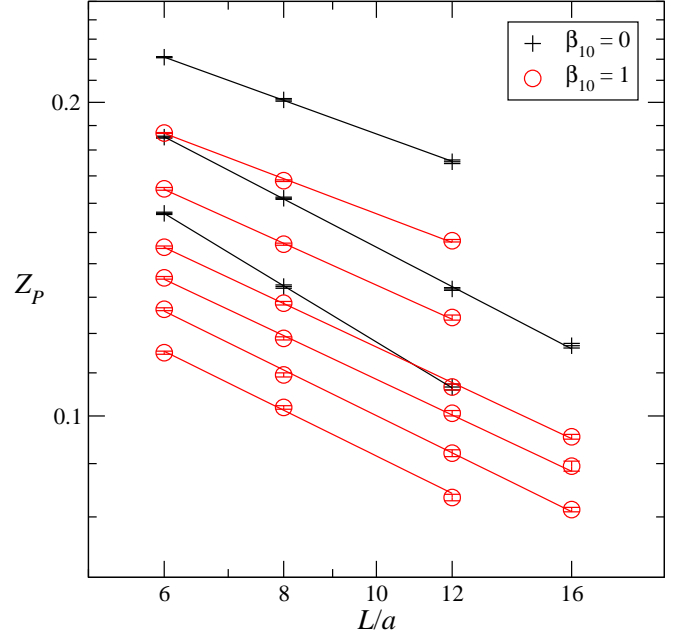$$\log Z_P(L/a) = c_0 + c_1 \log L/8a + c_2(\log L/8a)^2. \qquad (15)$$

FIG. 6: The pseudoscalar renormalization constant Z_P vs. L/a (Table II). The crosses are from simulations with $\beta_{10} = 0$, $\beta = 10.0$ to 8.5. The circles are from simulations with $\beta_{10} = 1$: top to bottom, $\beta = 7.0$ to 3.5. The straight lines are fits to each set of points at given (β, β_{10}); the slope gives γ_m.
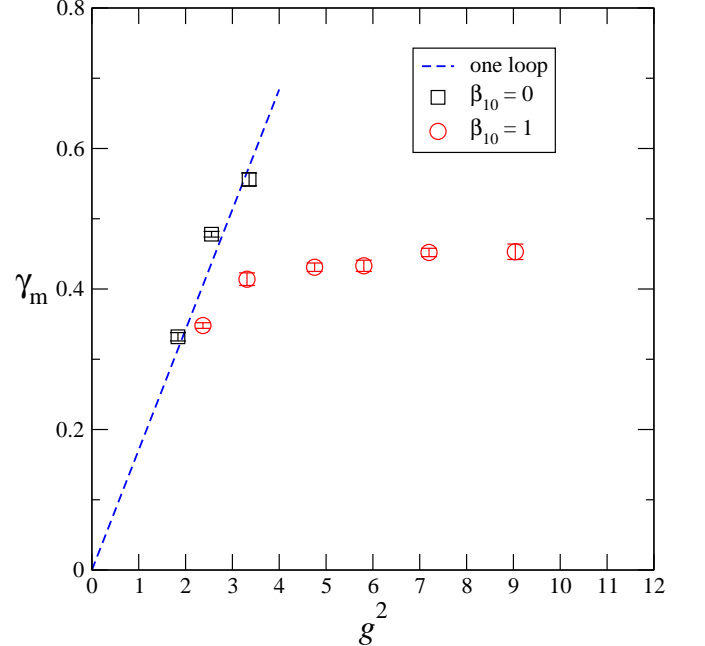

FIG. 7: Mass anomalous dimension $\gamma(g^2)$ from the linear fits shown in Fig. 6, plotted against $g^2(L = 8a)$. The squares are from the $\beta_{10} = 0$ data while the circles are from $\beta_{10} = 1$. The line is the one-loop result.
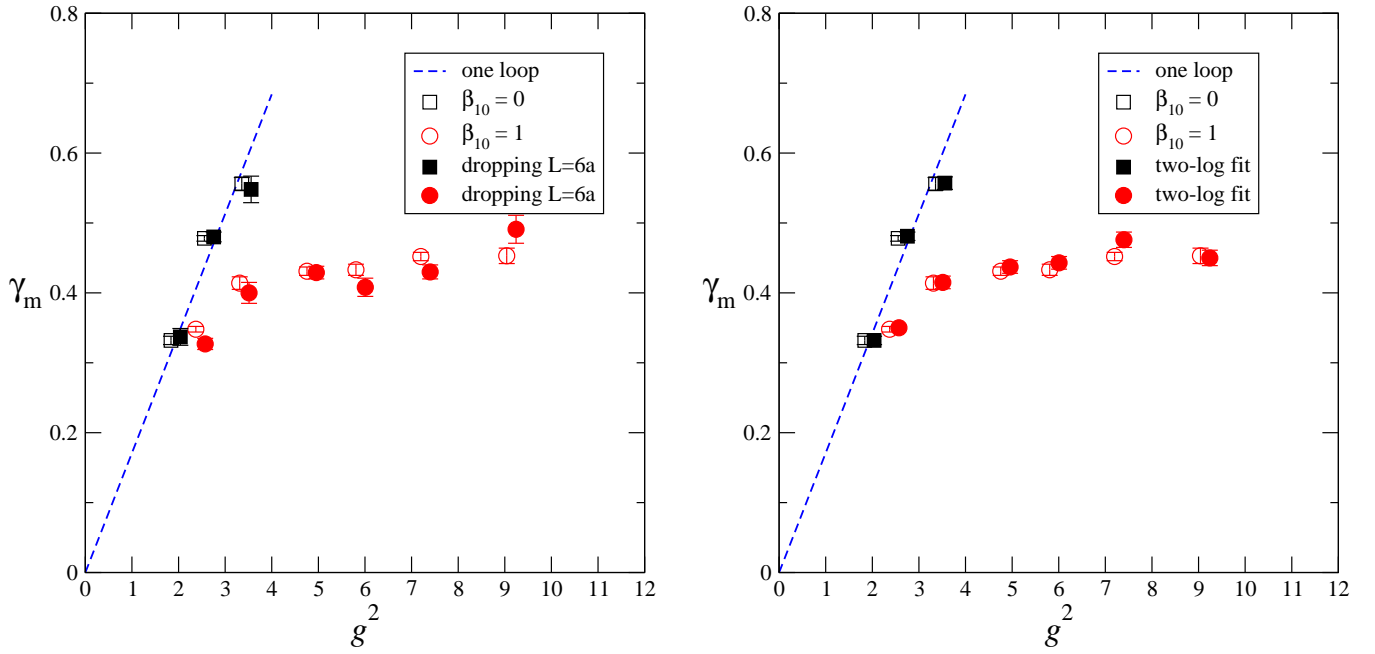
FIG. 8: Comparison of different fit types. Empty symbols as in Fig. 7. Left panel: full symbols derive from linear fits in which the $L = 6a$ points are omitted. Right panel: full symbols derive from fits to Eq. (15), in which a $\log^2$ term has been added. Results are plotted against $g^2(L = 8a)$. The filled symbols have been slightly displaced to the right.

In all cases the mass anomalous dimension at $g^2(L = 8a)$ is given by $-c_1$. We show a comparison of the different fit types in Fig. 8, plotted against the running coupling $g^2(L = 8a)$. It is apparent that the result for $\gamma_m(g^2)$ is quite robust under variations in the fitting procedure. While some of the linear fits to all volumes give high χ^2, dropping the $L = 6a$ points brings χ^2 under control.[6]

A comparison of $\beta_{10} = 0$ to $\beta_{10} = 1$ shows that there is some disagreement. Of the points obtained with $\beta_{10} = 1$, only the weakest-coupling point is in agreement with the results of $\beta_{10} = 0$ simulations. The two strongest-coupling points obtained with $\beta_{10} = 0$ lie far above the line connecting the $\beta_{10} = 1$ points. The former originate from simulations near the strong-coupling transition of the $\beta_{10} = 0$ theory. This is a lattice artifact, pushed off to stronger couplings by the introduction of $\beta_{10} > 0$. Thus the disagreement between the two sets of points should be settled in favor of the $\beta_{10} = 1$ points.

All our fits show that γ_m departs from the one-loop line and levels off at $\gamma_m \simeq 0.45$ at strong coupling. The highest point in Fig. 8 gives us the bound $\gamma_m < 0.51$.

---

[6] There are two $\beta_{10} = 1$ points with high χ^2 where dropping $L = 6a$ leaves no degrees of freedom to the fit. One is the weakest-coupling point; it sits near the one-loop curve and agrees with the corresponding $\beta_{10} = 0$ point, so we do not concern ourselves with it further. The other is the point at the strongest coupling, where $\chi^2/\text{dof} = 5/1$ before dropping $L = 6a$.

V. COMPARISON OF SU(2), SU(3), AND SU(4) THEORIES

The present paper describes one of a set of three related theories, which differ only in their color content. The obvious way to compare these systems uses the language of large N. The 't Hooft coupling is $\lambda = g^2 N$ and in large N we expect to see collapse of data for different values of N onto a common function of λ, up to $O(1/N)$ corrections.

For theories with $N_f = 2$ fermions in the two-index symmetric representation, the renormalization group equation takes the form

$$\frac{d\lambda}{d\log\mu} = -\frac{b_1}{N}\lambda^2 - \frac{b_2}{N^2}\lambda^3 + \cdots \qquad (16)$$

where each of the terms on the right hand side is $O(N^0)$,

$$\frac{b_1}{N} = \frac{1}{16\pi^2}\left(\frac{7}{3} - \frac{8}{3N}\right), \qquad (17)$$

$$\frac{b_2}{N^2} = \left(\frac{1}{16\pi^2}\right)^2\left[\frac{2}{3} + O\left(\frac{1}{N}\right)\right]. \qquad (18)$$

The large-N limit of these systems has no IRFP in two-loop order, since $b_2 > 0$. The one-loop mass anomalous dimension at $N = \infty$ is

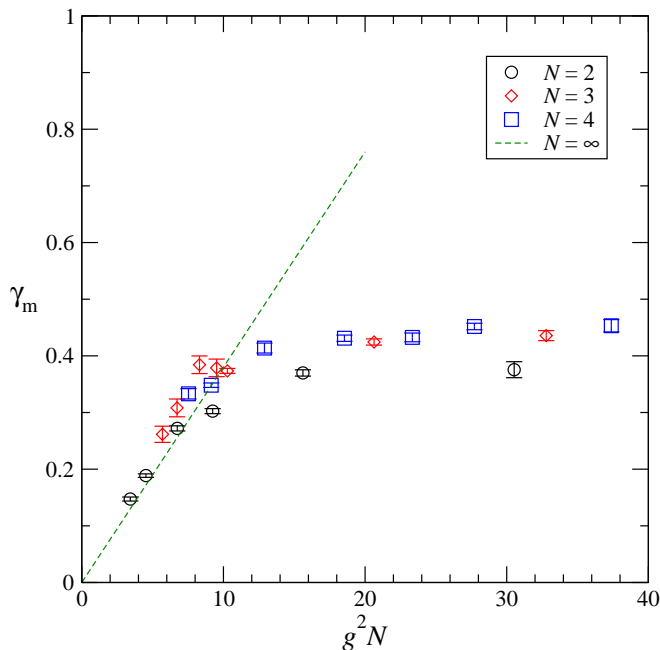$$\gamma_m = \frac{6}{16\pi^2}\lambda. \qquad (19)$$

FIG. 9: γ_m for the SU(2), SU(3), and SU(4) theories displayed as a function of $\lambda = g^2 N$ where g^2 is the Schrödinger functional coupling. The line is the lowest order large-N prediction, Eq. (19). For SU(3), we have dropped two strong-coupling points calculated with $\beta_6 = 0$, since they are superseded by $\beta_6 = 0.5$ data; likewise for SU(4), where two $\beta_{10} = 0$ points have been dropped (cf. Fig. 7).
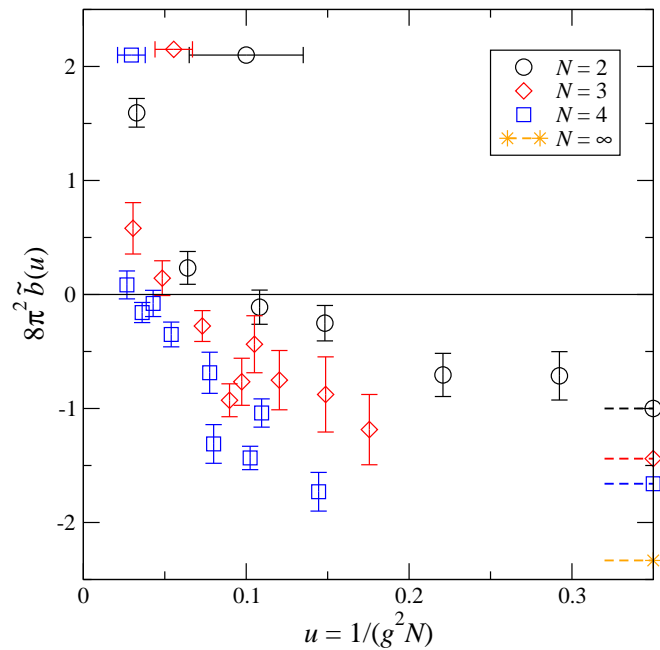
FIG. 10: Beta functions for the SU(2), SU(3), and SU(4) theories displayed à la large N [Eq. (20)]. The dashed lines at the right edge of the picture mark the weak-coupling limit as predicted by the one-loop coefficient, Eq. (17). The points with horizontal error bars mark each beta function's estimated zero (if it exists).

We collect our data from $N = 2$, 3, and 4 and plot them against λ, taking g^2 to be the Schrödinger functional coupling. For clarity, we use only the results of the linear fits, Eqs. (8) and (14), that do *not* drop $L = 6a$.

We begin this time with γ_m, plotted in Fig. 9. We have already noted that all three theories give results for γ_m that follow the one-loop line in weak coupling. Since the rescaled Casimir operators $C_2(R)/N$ for the three theories are similar (1, 10/9, 9/8) and close to the large-N value $[1 + O(1/N)]$, the ascending parts of the curves indeed almost coincide. What is remarkable is that all three theories fall off the one-loop line and level off in the neighborhood of $\gamma_m = 0.4$. This is a new regime of large-N scaling behavior.

The beta function, displayed in Fig. 10, shows similar trends. In analogy with Eq. (7), we define

$$\tilde{b}(1/\lambda) \;=\; \frac{d(1/\lambda)}{d \log L} = \frac{1}{N}\tilde{\beta}(1/g^2) \qquad (20)$$

$$= -\frac{2b_1}{N} - \frac{2b_2}{N^2}\lambda + \cdots, \qquad (21)$$

and we plot it against $u = 1/\lambda$. For our small values of N, the leading correction to b_1 is large, and so the weak coupling limits of the beta functions for different values of N do not coincide. We have shown the limiting behavior for each N on the right edge of Fig. 10, along with the

limiting value $-7/(24\pi^2)$ [Eq. (17)]. Our results, along with their (possible) fixed points, march leftwards as N increases. The $N = 2$ IRFP lies at $1/\lambda = 0.100(35)$. The existence of transitions for $N = 3$ and 4 is more uncertain, but our fits put them at $1/\lambda$ in the range 0.044–0.067 and 0.021–0.038, respectively. It is certainly plausible to imagine that all three theories have IRFP's, and their location moves to ever stronger coupling as N increases. The two-loop beta function predicts that the IRFP has to disappear for N sufficiently large (at $N \simeq 37$). We cannot rule out that by $N = 3$ this has already happened.

VI. CONCLUSIONS

We began our study of these related models hoping to answer two questions:

1. Do the systems exhibit walking, or do they possess an IRFP?

2. How large does the mass anomalous dimension get?

We were able to answer the first question cleanly for $N = 2$: there is an IRFP. For larger N, the situation remains less clear: if there is an IRFP, it moves to ever stronger coupling as N increases, where simulations become ever more difficult.

Qualitatively, the dynamics of all three models are dominated by their slow running. (This could have been anticipated simply by examining the two-loop beta function.) This makes the models quite different from conventional QCD with small N_f. Slow running was the key that allowed us to measure the mass anomalous dimension. In all cases, γ_m remained less than about 0.45 over the observed range. This observation alone, independent of the existence of an IRFP, renders the theories unsuitable as candidates for phenomenologically viable walking technicolor models.

We are struck by the fact that, for all three theories, the two-loop beta function, expressed in terms of the Schrödinger functional coupling, does an excellent job of reproducing our observed beta functions. At the same time, the behavior of the mass anomalous dimension is quite different from the perturbative prediction, and is universal—for all three theories γ_m falls off the one loop formula and becomes (nearly) constant, independent of the value of the renormalized gauge coupling.

Appendix A: nHYP smearing for SU(4)

1. Smearing and normalization

The formulas of nHYP smearing, introduced in Ref. [33], are given in detail in Ref. [34] for the SU(2) and SU(3) gauge groups. The smeared links $V_{n\mu}$ are constructed from the bare links $U_{n\mu}$ in three consecutive smearing steps via intermediate fields $\widetilde{V}$ and $\overline{V}$ according to

$$V_{n\mu} = \mathrm{Proj}_{\mathrm{U}(N)} \left[(1-\alpha_1)U_{n\mu} + \frac{\alpha_1}{6} \sum_{\pm\nu\neq\mu} \widetilde{V}_{n\nu;\mu} \widetilde{V}_{n+\hat{\nu},\mu;\nu} \widetilde{V}^{\dagger}_{n+\hat{\mu},\nu;\mu} \right], \tag{A1a}$$

$$\widetilde{V}_{n\mu;\nu} = \mathrm{Proj}_{\mathrm{U}(N)} \left[(1-\alpha_2)U_{n\mu} + \frac{\alpha_2}{4} \sum_{\pm\rho\neq\nu,\mu} \overline{V}_{n\rho;\nu\,\mu} \overline{V}_{n+\hat{\rho},\mu;\rho\,\nu} \overline{V}^{\dagger}_{n+\hat{\mu},\rho;\nu\,\mu} \right], \tag{A1b}$$

$$\overline{V}_{n\mu;\nu\,\rho} = \mathrm{Proj}_{\mathrm{U}(N)} \left[(1-\alpha_3)U_{n\mu} + \frac{\alpha_3}{2} \sum_{\pm\eta\neq\rho,\nu,\mu} U_{n\eta} U_{n+\hat{\eta},\mu} U^{\dagger}_{n+\hat{\mu},\eta} \right]. \tag{A1c}$$

Here the restricted sums ensure that only links that share a hypercube with $U_{n\mu}$ enter the smearing. The parameters α_i offer an arena for optimization but we retained the choice $(0.75, 0.6, 0.3)$ of Refs. [33, 34], reasoning that the coefficients are geometric in nature and hence shouldn't change much when the gauge group is changed. The projection to U(N) indicated in Eqs. (A1) is of course dependent on the gauge group. This is the normalization, the "n" in nHYP.

We accomplish the projection by an extension of the method of Ref. [34] to SU(4). Use of the Cayley–Hamilton theorem gives a formula that can be differentiated later to obtain the force for the molecular-dynamics evolution. Given a general 4×4 matrix Ω, the projected matrix V is given by

$$V = \Omega(\Omega^{\dagger}\Omega)^{-1/2}. \tag{A2}$$

This requires calculation of the inverse square root of $Q \equiv \Omega^{\dagger}\Omega$, which is a positive Hermitian matrix. Presuming Q to be non-singular, the Cayley–Hamilton theorem allows us to write $Q^{-1/2}$ as a polynomial in Q,

$$Q^{-1/2} = f_0 + f_1 Q + f_2 Q^2 + f_3 Q^3. \tag{A3}$$

We use a Jacobi algorithm to solve for the eigenvalues g_i of Q. (We will not need derivatives of g_i so they need

not be found analytically.) By writing Eq. (A3) in the eigenbasis of Q we obtain a linear system for f_i,

$$
\begin{pmatrix}
1 & g_0 & g_0^2 & g_0^3 \\
1 & g_1 & g_1^2 & g_1^3 \\
1 & g_2 & g_2^2 & g_2^3 \\
1 & g_3 & g_3^2 & g_3^3
\end{pmatrix}
\begin{pmatrix}
f_0 \\ f_1 \\ f_2 \\ f_3
\end{pmatrix}
=
\begin{pmatrix}
g_0^{-1/2} \\ g_1^{-1/2} \\ g_2^{-1/2} \\ g_3^{-1/2}
\end{pmatrix}. \qquad \text{(A4)}
$$

This system can also be solved numerically; since, however, we will need to differentiate the result, we solve it analytically by inverting the Vandermonde matrix. The solutions f_i are rational functions of $r_i \equiv \sqrt{g_i}$ or, more conveniently, of the symmetric polynomials

$$
\begin{aligned}
u &= r_0 + r_1 + r_2 + r_3 & \text{(A5a)} \\
v &= r_0 r_1 + r_0 r_2 + r_0 r_3 + r_1 r_2 + r_1 r_3 \\
& \quad + r_2 r_3 & \text{(A5b)} \\
w &= r_0 r_1 r_2 + r_0 r_1 r_3 + r_0 r_2 r_3 + r_1 r_2 r_3 & \text{(A5c)} \\
x &= r_0 r_1 r_2 r_3. & \text{(A5d)}
\end{aligned}
$$

Denoting a common denominator by

$$
\Delta = x \left(u^2 x - uvw + w^2 \right), \qquad \text{(A6)}
$$

we have $f_i = N_i/\Delta$, where

$$
\begin{aligned}
N_0 &= u^2 wx - u \left(-v^2 x + vw^2 + x^2 \right) - vwx \\
& \quad + w^3 & \text{(A7a)} \\
N_1 &= u^3 x - 2u^2 vw + u \left(v^3 + 2w^2 \right) \\
& \quad - w \left(v^2 + x \right) & \text{(A7b)} \\
N_2 &= -u^3 v + u^2 w - u \left(x - 2v^2 \right) - 2vw & \text{(A7c)} \\
N_3 &= uv - w. & \text{(A7d)}
\end{aligned}
$$

This completes the calculation of the quantities needed to normalize Ω.

2. Force in molecular dynamics

We follow still the derivation in Sec. 3 of Ref. [34], which is based on Morningstar and Peardon [42].

The force is the derivative of the effective action with respect to simulation time τ. The first step is to note that the fermionic part of the action includes only the fat links $V_{n\mu}$, so

$$
\frac{d}{d\tau} S_{\text{eff}} = \operatorname{Re} \operatorname{tr} \frac{\delta S_{\text{eff}}}{\delta V_\mu} \frac{dV_\mu}{d\tau} \equiv \operatorname{Re} \operatorname{tr} \left(\Sigma_{n\mu} \dot{V}_{n\mu} \right). \qquad \text{(A8)}
$$

One proceeds to apply the chain rule repeatedly to $\dot{V}_{n\mu}$ via Eqs. (A1) until one arrives at derivatives $\dot{U}_{n\mu}$ of the thin links.[7] The only factor in the chain rule that

---

[7] In fact the chain rule is first applied to the change of representation from decuplet to fundamental; this is followed by the fat-link chain rule.

depends on the group comes from the U(N) projection (A2), which appears at every level of smearing in Eqs. (A1). In order to write a derivative $\dot{V}$ in terms of $\dot{\Omega}$, we use the Cayley–Hamilton formula (A3) [cf. Eq. (3.10) of Ref. [34]],

$$
\begin{aligned}
\operatorname{Re} \operatorname{tr} \Sigma \dot{V} &= \operatorname{Re} \operatorname{tr} \left[\Sigma \frac{d}{d\tau} (\Omega Q^{-1/2}) \right] \\
&= \operatorname{Re} \operatorname{tr} (Q^{-1/2} \Sigma \dot{\Omega}) + \operatorname{tr} (\Sigma \Omega) \dot{f}_0 + \operatorname{tr} (Q \Sigma \Omega) \dot{f}_1 \\
& \quad + \operatorname{tr} (Q^2 \Sigma \Omega) \dot{f}_2 + \operatorname{tr} (Q^3 \Sigma \Omega) \dot{f}_3 + f_1 \operatorname{tr} (\Sigma \Omega \dot{Q}) \\
& \quad + f_2 \operatorname{tr} [(\Sigma \Omega Q + Q \Sigma \Omega) \dot{Q}] + f_3 \operatorname{tr} [(\Sigma \Omega Q^2 \\
& \quad + Q \Sigma \Omega Q + Q^2 \Sigma \Omega) \dot{Q}].
\end{aligned}
$$
$$\text{(A9)}$$

Upon defining the traces

$$
c_n = \frac{1}{n+1} \operatorname{tr} Q^{n+1}, \qquad \text{(A10)}
$$

one can write

$$
\dot{f}_i = \sum_{n=0}^{3} b_{in} \operatorname{tr} \left(Q^n \dot{Q} \right). \qquad \text{(A11)}
$$

where $b_{in} = \partial f_i / \partial c_n$. Then

$$
\operatorname{Re} \operatorname{tr} \Sigma \dot{V} = \operatorname{Re} \operatorname{tr} (Q^{-1/2} \Sigma \dot{\Omega}) + \operatorname{Re} \operatorname{tr} A \dot{Q}, \qquad \text{(A12)}
$$

where

$$
\begin{aligned}
A &= \sum_{n=0}^{3} \operatorname{tr} (B_n \Sigma \Omega) Q^n + f_1 \Sigma \Omega + f_2 (\Sigma \Omega Q + Q \Sigma \Omega) \\
& \quad + f_3 (\Sigma \Omega Q^2 + Q \Sigma \Omega Q + Q^2 \Sigma \Omega), \qquad \text{(A13)}
\end{aligned}
$$

with $B_n = b_{0n} + b_{1n} Q + b_{2n} Q^2 + b_{3n} Q^3$. Now we differentiate $Q = \Omega^\dagger \Omega$ to obtain finally

$$
\operatorname{Re} \operatorname{tr} \Sigma \dot{V} = \operatorname{Re} \operatorname{tr} \left[(Q^{-1/2} \Sigma + A \Omega^\dagger + A^\dagger \Omega^\dagger) \dot{\Omega} \right]. \quad \text{(A14)}
$$

The derivatives b_{ij} are calculated via the eigenvalues g_k through the chain rule,

$$
b_{ij} = \frac{\partial f_i}{\partial c_j} = \sum_k \frac{\partial f_i}{\partial g_k} \frac{\partial g_k}{\partial c_j}. \qquad \text{(A15)}
$$

The matrix $\partial g_k / \partial c_j$ is the inverse of the Vandermonde matrix $\partial c_k / \partial g_j = (g_j)^k$, so that we still don't need an analytical expression for the eigenvalues. The derivatives $\partial f_i / \partial g_k$ can be calculated directly from the above expressions for f_i. The final result for b_{ij} can, like the f_i, be written as rational functions of the symmetric polynomials u, v, w, x. The expressions are lengthy and not particularly illuminating [43].

Appendix B: Tests of soft gauge actions

In lowest order, the action of Eq. (3) is just a quadratic form in the vector potentials of the thin and fat links. In momentum space the fat link's gauge field $B_\mu(q)$ is related to the thin link's gauge field $A_\mu(q)$ through a form factor $\tilde{h}_{\mu\nu}(q)$ whose specific form depends on the particular definition of the fat link,

$$B_\mu(q) = \sum_\nu \tilde{h}_{\mu\nu}(q) A_\nu(q). \tag{B1}$$

In general, $\tilde{h}_{\mu\nu}(q) \sim 1 + O(a^2 q^2) + O(a^4 q^4) + \cdots$.

Let us generalize to N colors, with an ordinary plaquette term made of thin link plus a closed loop made of fat links in representation R of the gauge group. We can write the quadratic gauge action as

$$
\begin{aligned}
S_0^G &= -\frac{1}{2g_0^2} \int_{pp'} (2\pi)^4 \delta^4(p + p') \\
&\quad \times \big[(1-s) A_\mu(p') D_{\mu\nu}^{\text{thin}}(p) A_\nu(p) \\
&\quad + s B_\mu(p') D_{\mu\nu}^{\text{fat}}(p) B_\nu(p)\big],
\end{aligned}
\tag{B2}
$$

where D^{thin} is the thin link kernel and D^{fat} is the fat link kernel. (We have suppressed color indices.) In practice, we will use a plaquette fat link term, so $D^{\text{fat}} = D^{\text{thin}}$. The bare coupling is

$$\frac{1}{g_0^2} = \frac{\beta}{N} T(f) + \frac{\beta_R}{d_R} T(R), \tag{B3}$$

where $T(f) = 1/2$ is the trace normalization of the fundamental representation while $T(R)$ is that of the representation R; $d(R)$ is the dimension of the latter. We also define $s = x/(1+x)$ where

$$x = \frac{\beta_R T(R)/d_R}{\beta T(f)/N}. \tag{B4}$$

In SU(4) with decuplet fat links, $x = \frac{12}{5} \beta_R/\beta$.

Upon using Eq. (B1), we find the free gauge boson action to be

$$S_0^G = -\frac{1}{2g_0^2} \int_{pp'} (2\pi)^4 \delta^4(p + p') \left[A_\mu(p') D_{\mu\nu}(p) A_\nu(p)\right], \tag{B5}$$

where

$$D_{\mu\nu} = (1-s) D_{\mu\nu}^{\text{thin}} + s \tilde{h}_{\rho\mu} D_{\rho\sigma}^{\text{fat}} \tilde{h}_{\sigma\nu}. \tag{B6}$$

After adding a gauge fixing term,

$$S_{\text{gf}} = -\frac{1}{2g_0^2} \sum_{\mu\nu} \int_k \text{Tr}\, \frac{1}{\xi} \hat{k}_\mu \hat{k}_\nu A_\mu(-k) A_\nu(k), \tag{B7}$$

where $\hat{k}_\mu = (2/a)\sin(ak_\mu/2)$, the gauge boson propagator is found by inverting the field equation,

$$\sum_\nu \left[\frac{1}{\xi} \hat{k}_\mu \hat{k}_\nu + D_{\mu\nu}(k)\right] G_{\nu\tau}(k) = \delta_{\mu\tau}. \tag{B8}$$

The case of a Wilson action and APE smearing can be treated analytically. In that case both the action and smearing are built out of projectors,

$$P_{\mu\nu}^T = \delta_{\mu\nu} - \frac{\hat{k}_\mu \hat{k}_\nu}{\hat{k}^2}, \qquad P_{\mu\nu}^L = \frac{\hat{k}_\mu \hat{k}_\nu}{\hat{k}^2}. \tag{B9}$$

The Wilson gauge action is

$$D_{\mu\nu}(k) = \hat{k}^2 P_{\mu\nu}^T, \tag{B10}$$

and the APE smearing term is [44]

$$\tilde{h}_{\mu\nu}(q) = f(q) P_{\mu\nu}^T + P_{\mu\nu}^L, \tag{B11}$$

with $f(q) = 1 - (\alpha/6)\hat{q}^2$; α is the smearing parameter. This means that the soft APE-smeared Wilson action is

$$D_{\mu\nu}(k) = (1 - s + sf^2) \hat{k}^2 P_{\mu\nu}^T \tag{B12}$$

and thus the propagator is

$$G_{\mu\nu}(k) = \frac{1}{\hat{k}^2} \left[\frac{1}{1 - s + sf^2} P_{\mu\nu}^T + \xi P_{\mu\nu}^L\right]. \tag{B13}$$

More complicated actions and smearing do not have this projector form, and the final result for $G_{\mu\nu}(k)$ is not illuminating.

So much for the gluon propagator. The second ingredient needed for perturbative calculations is the fermion–gauge boson vertex. In a fat action with unitary links it is simply the smearing form factor multiplied by the unsmeared vertex Γ_ν,

$$\tilde{\Gamma}_\mu = \Gamma_\nu \tilde{h}_{\nu\mu}. \tag{B14}$$

All Feynman graphs with an internal gluon line are built of the combination of terms

$$\tilde{G}_{\mu\nu}(k) = \tilde{\Gamma}_\mu G_{\mu\nu}(k) \tilde{\Gamma}_\nu = \Gamma_\nu [\tilde{h}_{\nu\mu} G_{\mu\rho} \tilde{h}_{\sigma\rho}] \Gamma_\sigma \tag{B15}$$

and so for all practical purposes, the gluon propagator $G_{\mu\nu}(k)$ is just replaced by the combination $\tilde{h}_{\nu\mu} G_{\mu\rho} \tilde{h}_{\sigma\rho}$. For APE smearing on top of the Wilson gauge action, this replacement can be performed analytically, and the transverse part of the propagator times form factors is just the usual Wilson propagator, rescaled by the factor

$$\frac{f^2(q)}{1 - s + sf^2(q)}. \tag{B16}$$

Let us recall some features of perturbation theory with fat links. Consider first the usual smeared fermion action with unsmeared gauge action, $s = 0$. The good features of this action arise because the form factor in Eq. (B16) suppresses the large-q part of loop integrals. This shrinks the size of tadpole graphs and lowers the size of one loop matching factors. A positive weight s increases the form factor at large q, and a negative s effectively amounts to increased smearing.
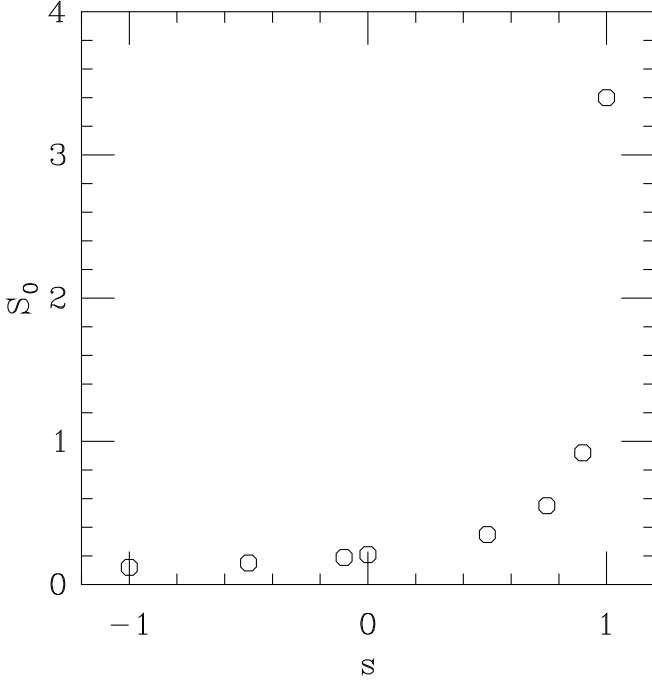
FIG. 11: Additive mass renormalization [see Eq. (B17)] for nHYP clover fermions with $c_{SW} = 1$ as a function of the relative weight s of thin- and fat- link terms.
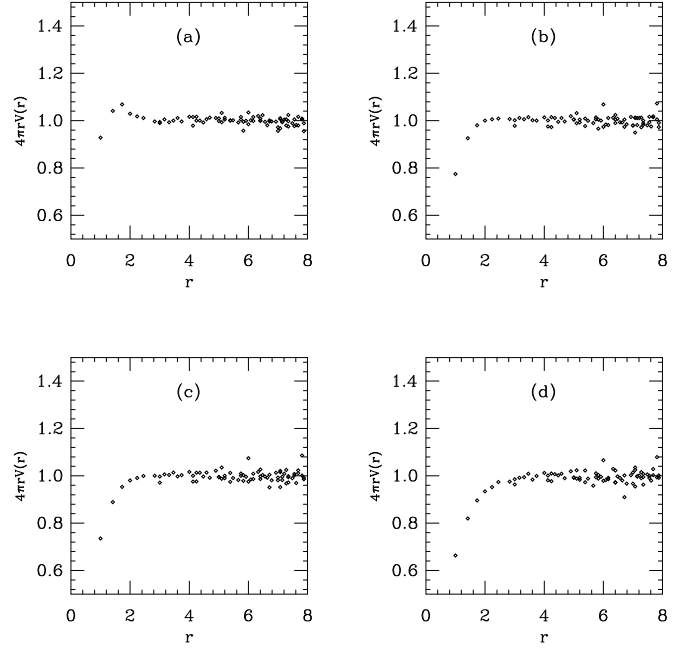

FIG. 12: $4\pi r V(r)$, the tree-level static potential due to a soft Wilson action and seen by nHYP-smeared sources, at four s values: (a) $s = 0.7$, (b) $s = 0.2$, (c) $s = 0$, (d) $s = -0.5$.

The case $s = 1$ is peculiar in that the effects of smearing are completely undone. What is happening in this case is that the transformation $A \to B$ is just a field redefinition: we are doing Monte Carlo with the fat link everywhere as the fundamental gauge field. Only if the gauge action is smeared differently from the vertex can smearing achieve its goal.

One way to reduce the value of the effective gauge boson propagator at large q is to make s negative. Then the fat term amounts to a further smearing of the effective quark–gluon vertex. This might be a feature worth exploring in low-N_f situations.

As described in the main body of the paper, we have chosen $s > 0$ for a nonperturbative reason, and so we should check if this choice is benign from the point of view of perturbation theory. We show the results for two observables to check this point.

Fig. 11 shows the additive mass renormalization for nHYP clover fermions with $c_{SW} = 1$, parametrized as

$$\delta m = \frac{g_0^2}{4\pi} 2T(R)S_0. \qquad (B17)$$

(The choice of factors is taken to make the case of fundamental representation fermions most transparent.) The $s = 1$ case reduces to the thin link value. The undoing of smearing is quite abrupt, and nearly any value away from $s = 1$ produces a large suppression of δm.

In perturbation theory, the tree level static potential between point sources is Coulombic, up to lattice arti- facts:

$$\hat{V}(r) = g^2 C_F V(r) \sim g^2 C_F \frac{1}{4\pi r} . \qquad (B18)$$

When the sources are themselves nHYP-smeared, the short distance part of the potential is softened. This is a usual consequence of smearing [45]. Fig. 12 shows $4\pi r V(r)$ for soft actions with several choices of s. It appears that from the point of view of perturbation theory, the soft gauge action does not obviously harm useful properties of the lattice action.

Finally, the simulations we are performing with the soft action are done at rather strong coupling. In this regime, perturbation theory does not reliably predict the observed additive mass renormalization. This is shown indirectly in Fig. 13, a plot of κ_c against the bare coupling $8/g_0^2 = \beta + \frac{12}{5}\beta_{10}$. Different plotting symbols show different values of β_{10}. In weak coupling the observed additive mass renormalization qualitatively agrees with what is shown in Fig. 11: larger β_{10}/β produces larger additive mass renormalization. However, in strong coupling the effect reverses. One cannot help speculating that there is a connection between a large value of κ_c and a nearby first order transition, and that when κ_c falls, the transition has moved away.

Appendix C: Ensembles

Our algorithm is the hybrid Monte Carlo (HMC) algorithm of Duane and Kogut [46–48]. We accelerate the
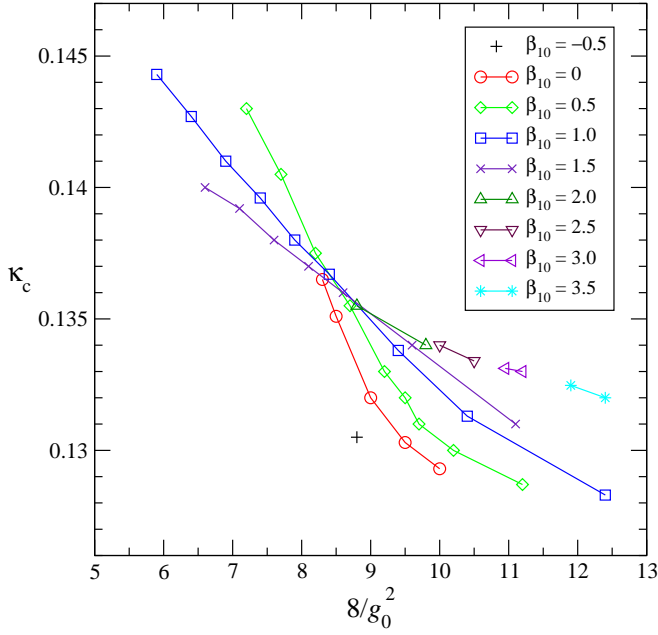
FIG. 13: Dependence of κ_c on bare coupling $8/g_0^2 = \beta + \frac{12}{5}\beta_{10}$, for various values of β_{10}.

molecular dynamics integration with an additional heavy pseudo-fermion field as suggested by Hasenbusch [49], with multiple time scales [50], and with a second-order Omelyan integrator [51]. Lattice sizes range from 6^4 to 16^4 sites.

We list in Table III the values of $(\beta, \beta_{10}, \kappa_c)$ and the number of trajectories run at each volume, along with the length of the trajectories and the acceptance. Poor acceptance forced us to shorten the trajectory length in many cases from the usual value of 1.

The observables we measure are the (inverse) Schrödinger-functional running coupling, $1/g^2$, and the pseudoscalar renormalization factor, Z_P. (We measure Z_P on the same configurations used to determine $1/g^2$.) Both of them turn out to have long autocorrelations. We monitored and controlled this problem by running 4 or 8 streams in parallel at each (β, β_{10}) and L. After analyzing each stream separately, we fit the results of the streams together to a constant. We demanded that the χ^2/dof of the constant fit not exceed 6/3 for 4 streams, or 10/7 for 8 streams. For the largest volume $L = 16a$ at $(\beta, \beta_{10}) = (5, 1)$, we were not able to overcome the autocorrelations in $1/g^2$. We therefore omit this point from the analysis of the running coupling. The autocorrelations in Z_P, on the other hand, did allow a consistent determination, and thus we keep this point in the analysis of the mass anomalous dimension.

TABLE III: Ensembles generated at the bare couplings $(\beta, \beta_{10}, \kappa_c)$ for the lattice sizes L used in this study. Listed are the total number of trajectories for all streams at given (β, β_{10}) and L, the trajectory length, and the HMC acceptance.

β	β_{10}	κ_c	L/a	trajectories (thousands)	trajectory length	acceptance
10.0	0	0.1293	6	19.6	1.0	0.97
			8	6.9	1.0	0.95
			12	4.8	1.0	0.94
9.0	0	0.13206	6	20.2	1.0	0.96
			8	8.1	1.0	0.95
			12	12.0	1.0	0.85
			16	5.4	1.0	0.78
8.5	0	0.1349	6	20.2	1.0	0.89
			8	13.6	1.0	0.78
			12	6.1	0.75	0.66
7.0	1	0.13361	6	48.8	1.0	0.95
			8	16.4	1.0	0.93
			12	10.3	1.0	0.68
6.0	1	0.13634	6	10.0	1.0	0.82
			8	20.0	0.5	0.88
			12	9.6	0.5	0.61
5.0	1	0.13912	6	8.6	1.0	0.55
			8	6.0	1.0	0.62
			12	12.5	0.5	0.48
			16	10.7	0.5	0.63
4.5	1	0.14055	6	8.6	1.0	0.52
			8	13.0	0.5	0.84
			12	10.6	0.5	0.56
			16	9.7	0.5	0.45
4.0	1	0.14193	6	9.4	1.0	0.58
			8	12.0	0.5	0.72
			12	16.2	0.5	0.43
			16	20.2	0.4	0.37
3.5	1	0.14318	6	14.6	1.0	0.53
			8	9.4	0.5	0.66
			12	19.2	0.25	0.64

[1] For reviews, see G. T. Fleming, PoS LATTICE **2008**, 021 (2008); E. Pallante, PoS LAT **2009**, 015 (2009); L. Del Debbio, PoS LATTICE **2010**, 004 (2010).

[2] For a review of the phenomenology, see C. T. Hill and E. H. Simmons, Phys. Rept. **381**, 235 (2003) [Erratum-ibid. **390**, 553 (2004)]

[3] W. E. Caswell, Phys. Rev. Lett. **33**, 244 (1974).

[4] T. Banks and A. Zaks, Nucl. Phys. B **196**, 189 (1982).

[5] Y. Shamir, B. Svetitsky and T. DeGrand, Phys. Rev. D **78**, 031502 (2008).

[6] T. DeGrand, Y. Shamir and B. Svetitsky, Phys. Rev. D **79**, 034501 (2009).

[7] T. DeGrand, Phys. Rev. D **80**, 114507 (2009).

[8] T. DeGrand, Y. Shamir, B. Svetitsky, Phys. Rev. **D82**, 054503 (2010).

[9] T. DeGrand, Y. Shamir, B. Svetitsky, Phys. Rev. **D83**, 074507 (2011).

[10] T. DeGrand, Y. Shamir, B. Svetitsky, PoS LATTICE **2011**, 060 (2011).

[11] T. DeGrand, Y. Shamir and B. Svetitsky, arXiv:1201.0935 [hep-lat].

[12] F. Sannino and K. Tuominen, Phys. Rev. D **71**, 051901 (2005).

[13] D. D. Dietrich and F. Sannino, Phys. Rev. D **75**, 085018 (2007).

[14] M. Lüscher, R. Narayanan, P. Weisz and U. Wolff, Nucl. Phys. B **384**, 168 (1992).

[15] M. Lüscher, R. Sommer, P. Weisz and U. Wolff, Nucl. Phys. B **413**, 481 (1994).

[16] S. Sint and R. Sommer, Nucl. Phys. B **465**, 71 (1996).

[17] K. Jansen and R. Sommer [ALPHA collaboration], Nucl. Phys. B **530**, 185 (1998) [Erratum-*ibid.* B **643**, 517 (2002)].

[18] M. Della Morte *et al.* [ALPHA Collaboration], Nucl. Phys. B **713**, 378 (2005).

[19] S. Sint and P. Weisz [ALPHA collaboration], Nucl. Phys. B **545**, 529 (1999).

[20] S. Capitani, M. Lüscher, R. Sommer and H. Wittig [ALPHA Collaboration], Nucl. Phys. B **544**, 669 (1999).

[21] M. Della Morte *et al.* [ALPHA Collaboration], Nucl. Phys. B **729**, 117 (2005).

[22] B. Lucini and G. Moraitis, Phys. Lett. B **668**, 226 (2008).

[23] T. Appelquist, G. T. Fleming and E. T. Neil, Phys. Rev. Lett. **100**, 171607 (2008) [Erratum-ibid. **102**, 149902 (2009)].

[24] T. Appelquist, G. T. Fleming and E. T. Neil, Phys. Rev. D **79**, 076010 (2009).

[25] A. J. Hietanen, K. Rummukainen and K. Tuominen, Phys. Rev. D **80**, 094504 (2009).

[26] F. Bursa, L. Del Debbio, L. Keegan, C. Pica and T. Pickup, Phys. Rev. D **81**, 014505 (2010).

[27] F. Bursa, L. Del Debbio, L. Keegan, C. Pica and T. Pickup, Phys. Lett. B **696**, 374 (2011).

[28] M. Hayakawa, K. -I. Ishikawa, Y. Osaki, S. Takeda, S. Uno and N. Yamada, Phys. Rev. D **83**, 074509 (2011).

[29] T. Karavirta, J. Rantaharju, K. Rummukainen and K. Tuominen, arXiv:1111.4104 [hep-lat]; arXiv:1201.2037 [hep-lat].

[30] T. Karavirta, K. Rummukainen and K. Tuominen, arXiv:1201.1883 [hep-lat].

[31] T. DeGrand and A. Hasenfratz, Phys. Rev. D **80**, 034506 (2009).

[32] B. Sheikholeslami and R. Wohlert, Nucl. Phys. B **259**, 572 (1985).

[33] A. Hasenfratz and F. Knechtli, Phys. Rev. D **64**, 034504 (2001).

[34] A. Hasenfratz, R. Hoffmann and S. Schaefer, JHEP **0705**, 029 (2007).

[35] Y. Iwasaki, K. Kanaya, S. Sakai and T. Yoshié, Phys. Rev. Lett. **69**, 21 (1992).

[36] Y. Iwasaki, K. Kanaya, S. Kaya, S. Sakai and T. Yoshié, Phys. Rev. D **69**, 014507 (2004).

[37] K. Nagai, G. Carrillo-Ruiz, G. Koleva and R. Lewis, Phys. Rev. D **80**, 074508 (2009).

[38] S. Catterall, J. Giedt, F. Sannino and J. Schneible, JHEP **0811**, 009 (2008).

[39] A. J. Hietanen, J. Rantaharju, K. Rummukainen and K. Tuominen, JHEP **0905**, 025 (2009).

[40] http://www.physics.utah.edu/~detar/milc/

[41] A. Hasenfratz, R. Hoffmann and S. Schaefer, Phys. Rev. D **78**, 054511 (2008).

[42] C. Morningstar and M. J. Peardon, Phys. Rev. D **69**, 054501 (2004) [hep-lat/0311018].

[43] See Supplemental Material at [URL will be inserted by publisher] for a *Mathematica* notebook for calculating f_i and b_{ij}, as well as a PDF file of the results.

[44] C. W. Bernard and T. A. DeGrand, Nucl. Phys. Proc. Suppl. **83**, 845 (2000) See also T. A. DeGrand, Phys. Rev. D **67**, 014507 (2003).

[45] A. Hasenfratz, R. Hoffmann and F. Knechtli, Nucl. Phys. Proc. Suppl. **106**, 418 (2002) [hep-lat/0110168].

[46] S. Duane and J. B. Kogut, Phys. Rev. Lett. **55**, 2774 (1985).

[47] S. Duane and J. B. Kogut, Nucl. Phys. B **275**, 398 (1986).

[48] S. A. Gottlieb, W. Liu, D. Toussaint, R. L. Renken and R. L. Sugar, Phys. Rev. D **35**, 2531 (1987).

[49] M. Hasenbusch, Phys. Lett. B **519**, 177 (2001).

[50] C. Urbach, K. Jansen, A. Shindler and U. Wenger, Comput. Phys. Commun. **174**, 87 (2006).

[51] T. Takaishi and P. de Forcrand, Phys. Rev. E **73**, 036706 (2006).